Modeling of the interaction of a volumetric metallic metamaterial structure with a relativistic electron beam

Xueying Lu,* Michael A. Shapiro, and Richard J. Temkin
Plasma Science and Fusion Center, Massachusetts Institute of Technology, Cambridge, Massachusetts 02139, USA
(Received 24 May 2015; published 18 August 2015)

We present the design of a volumetric metamaterial (MTM) structure and its interaction with a relativistic electron beam. This novel structure has promising applications in particle beam diagnostics, acceleration, and microwave generation. The volumetric MTM has a cubic unit cell allowing structures of arbitrary size to be configured as an array of identical cells. This structure allows the exploration of the properties of a metamaterial structure without having to consider substrates or other supporting elements. The dispersion characteristics of the unit cell are obtained using eigenmode simulations in the HFSS code and also using an effective medium theory with spatial dispersion. Good agreement is obtained between these two approaches. The lowest-order mode of the MTM structure is found to have a negative group velocity in all directions of propagation. The frequency spectrum of the radiation from a relativistic electron beam passing through the MTM structure is calculated analytically and also calculated with the CST code, with very good agreement. The radiation pattern from the relativistic electron beam is found to be backward Cherenkov radiation, which is a promising tool for particle diagnostics. Calculations are also presented for the application of a MTM-based wakefield accelerator as a possible all-metal replacement for the conventional dielectric wakefield structure. The proposed structure may also be useful for MTM-based vacuum electron devices for microwave generation and amplification.

DOI: 10.1103/PhysRevSTAB.18.081303 PACS numbers: 81.05.Xj, 41.60.Bq, 07.57.Hm, 41.75.Lx

I. INTRODUCTION

Metamaterials (MTMs) have been intensively studied in the microwave frequency range in recent years. MTMs are implemented as constitutive periodic structures with subwavelength unit cells, and they have novel features like negative refractive indices [1]. MTMs are promising to provide improved performance over traditional devices in the way that the unit cell design process allows more controllability and flexibility of electromagnetic characteristics, for example, dispersion [2,3]. Then we can build devices with interesting features and better performance by engineering the unit cell.

In the area of passive microwave devices, MTMs are applied to cloaking [4], "perfect" lens [5,6], antenna design [7], etc., and these MTMs are often based on 2D planar split ring resonators (SRRs) [2]. Research on high power microwave sources and particle accelerators can also benefit from introducing MTMs, and there are some pioneering studies on the interaction of an electron beam with MTMs [8–11]. The challenge of applying MTMs to active devices is that a design with planar unit cells naturally has the electromagnetic fields concentrated on the planar plates, so at the beam location, which must be at a distance away from the plates, field intensities are low. This makes it difficult to achieve a high coupling impedance with planar unit cells. Our work is new and different in the way that we are developing a real volumetric metallic 3D MTM structure from a cubic unit cell which can fill the full space automatically. Although volumetric MTM designs based on dielectric materials have been extensively studied, dielectric materials are less attractive for applications where electron beams propagate in vacuum through the MTM structure, such as in vacuum electron devices or accelerators. We can study the interaction of an electron beam with the 3D metallic MTM directly without a substrate supporting the MTM structure or other supporting parts.

Characterization of MTMs has aroused a lot of interest. Different methods have been developed to find the effective dielectric and magnetic parameters, such as the scattering parameter extraction method and the field averaging method [12–15]. These parameters are often scalar functions depending only on frequency, i.e., $\varepsilon(\omega)$ and $\mu(\omega)$. However, this model is not a good approximation outside the low-frequency range, since multipoles besides dipoles become important [16,17]. A parallel approach is to use a set of fields of $\mathbf{E}$, $\mathbf{D}$, and $\mathbf{B}$ with $\mathbf{D} = \varepsilon\mathbf{E}$, $\mathbf{B} = \mathbf{H}$, where ε is a tensor and depends on the frequency and the wave vector, $\varepsilon = \varepsilon(\omega, \mathbf{k})$. In this paper, we will use the latter approach. Demetriadou and Pendry [18] realized the role of spatial dispersion in longitudinal waves in 3D wires, though their

*xylu@mit.edu

goal was trying to minimize the dispersion. A successful modeling of surface waves on the interface of a wire array and vacuum using the spatial dispersion approach is presented by Shapiro *et al.* [19], and a discussion on the importance of spatial dispersion on polaritons with negative group velocity has been carried out by Agranovič and Gartstein [20].

Novel dispersion relations of the MTMs may give rise to unusual radiated waves from the electron beams. In conventional materials, when particles travel faster than the speed of light in the medium, Cherenkov radiation (CR) occurs. It is widely used in particle counters and position monitors [21]. In MTMs with negative group velocities, backward CR can be observed as first suggested by Veselago [1], and planar MTM structures aimed at generating backward radiation were developed [22] first in 2002. Both theoretical and experimental work [23–26] have verified backward CR using a phased antenna array to mimic a traveling current. The first experiment with a real electron beam was performed by Antipov *et al.* [9]. A waveguide loaded with SRRs and a wire array was built, and the measured frequency response of the incoming electron beam was in the negative-index band. Vorobev and Tyukhtin [27] calculated the CR generated by an electron bunch traveling perpendicular to a 2D wire array and found that radiation appears with an arbitrary charge velocity. The radiated field profile changes with different bunch lengths; thus, their discovery indicates a possible application of measuring beam bunch length and velocity using CR in MTMs.

In Sec. II, we will present the design of a unit cell with 3D negative group velocity. Section III presents the effective medium theory with spatial dispersion as an analytical model. Section IV presents the beam-wave interaction using the effective medium theory. Section V discusses the radiation pattern calculated using the CST code. Application of the structure as a wakefield accelerating source is discussed in Sec. VI, and conclusions are presented in Sec. VII.

II. UNIT CELL DESIGN

For the design of the metallic, volumetric MTM, we chose the unit cell to be a cube. We further chose to have an empty unit cell, with metallic capacitive and inductive elements arranged on the faces of the cube. Each face of the cube is identical to make the structure quasi-isotropic. To allow transmission of an electron beam, each face has a beam aperture in the center. To allow propagation of electromagnetic waves, each face has a set of four coupling slots, each about one-tenth of a wavelength, arranged symmetrically around the beam aperture. The detailed structure is shown in Fig. 1. The dimensions are chosen to put the operating frequency at around 17 GHz.

An eigenmode solver needs to be used to study the dispersion characteristics, and we chose the HFSS eigenmode solver to calculate the dispersion in the first Brillouin zone, as shown in Fig. 2(a). In (k_x, k_y, k_z) space, the

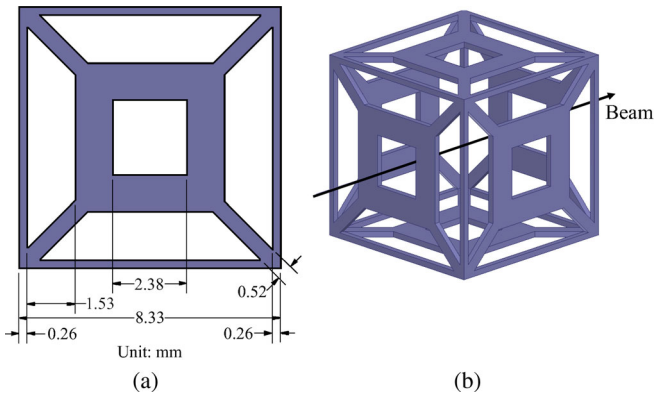

FIG. 1. Unit cell design geometry. (a) Face view. The thickness of each face is 0.26 mm. (b) 3D view. In later sections, we will introduce the electron beam that goes through the center of the beam holes of the cells lying on the beam line.

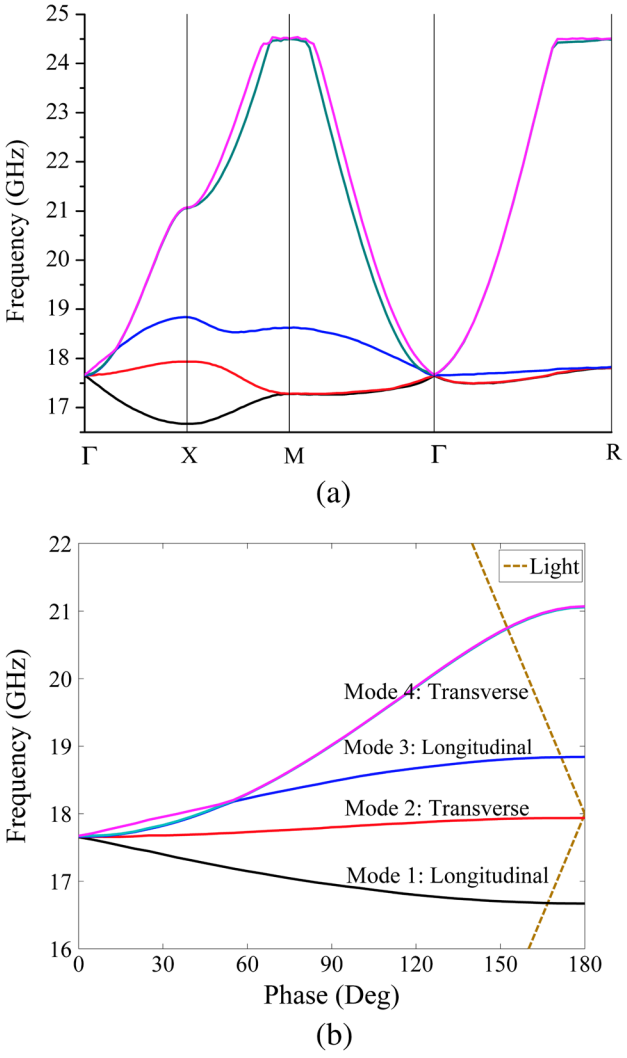

FIG. 2. Brillouin diagram of a unit cell. (a) Different regions in the first Brillouin zone. (b) $\Gamma - X$ region dispersion showing the intersection with the light line.

coordinates of the high symmetry points for a simple cubic lattice are $\Gamma(0,0,0)$, $X(\pi/p,0,0)$, $M(\pi/p,\pi/p,0)$, and $R(\pi/p,\pi/p,\pi/p)$, where p is the period of the unit cells.

We chose the specific parameters in Fig. 1 to make the structure balanced; i.e., all the modes have the same cutoff frequency at the Γ point. In this way, we can have dispersion curves with a greater slope; otherwise, the slope at the Γ point must be zero due to periodicity. Negative group velocity of the proposed unit cell is an inherent feature and is not critically dependent on a certain set of geometry parameters. For example, if we vary the size of the central square beam hole with the rest of the parameters unchanged, the fundamental mode (mode 1 in Fig. 2) will always have a negative group velocity in the $\Gamma - X$ region.

In the $\Gamma - X$ region, there are four modes, as in Fig. 2(b); among them, mode 1 and mode 3 are longitudinal. We are primarily interested in the longitudinal modes, which will strongly couple to an electron beam. Mode 2 and mode 4 are transverse modes that do not couple to the electron beam. Mode 4 is doubly degenerate with fields polarized in the y and z direction, respectively. In the X-M and $\Gamma - M$ regions, when the symmetry of the y and z directions is broken, mode 4 splits into two modes.

The electric field patterns of the longitudinal modes in the $\Gamma - X$ regions are shown in Fig. 3. In the eigenmode simulation, there is no electron beam, but finally we will put a relativistic beam into an array of the unit cells, where the beam lies on the axial line of the beam holes of the central-region unit cells, as denoted by the black arrows in Figs. 3(a) and 3(b). With the electron beam traveling at near the speed of light, the synchronized points of the beam and the longitudinal modes are 16.7 and 18.8 GHz. These are the points in Fig. 2(b) where the light line intersects mode 1 and 3, respectively. We will compare these frequencies calculated using the HFSS code with the frequencies calculated using the effective medium theory and the CST code later in this paper.

The quantitative axial electric fields at these synchronized points are shown in Fig. 3(d). Mode 1 has a field in the same direction within the same unit cell, while mode 3 has the opposite direction.

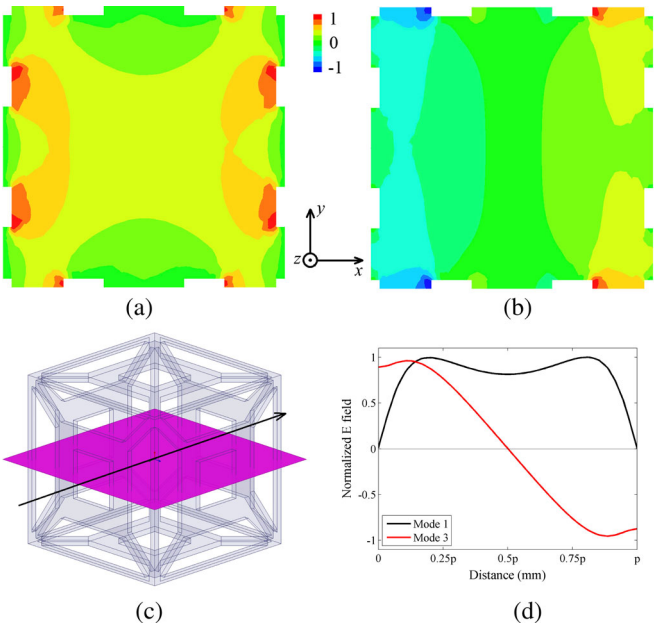

FIG. 3. Field patterns of the longitudinal eigenmodes in the $\Gamma - X$ region. The cutting plane is the middle plane going through the center of the beam hole. Black arrows denote possible beam paths for the purpose of later sections. Waves propagate to the right. The fields are shown on a linear scale. (a) Mode 1 (the negative index mode); y and z directions are symmetric. (b) Mode 3 (the positive index mode). (c) Cutting plane and future beam position. (d) Axial field patterns at the synchronized points with a relativistic beam at the speed of light.

III. EFFECTIVE MEDIUM THEORY WITH SPATIAL DISPERSION

One goal of this study is to investigate the interaction of an electron beam with the MTM medium. To get an analytical solution, we need to replace the actual structure of Fig. 1 with an effective medium. The effective medium model must agree well with the HFSS model for the dispersion characteristics. The effective medium theory aims to model subwavelength periodic structures with a continuous medium. It is a method of geometry simplification under the principle of keeping equivalent electromagnetic characteristics.

We will use the set of fields of **E**, **D**, and **B** with spatial dispersion. The tensor $\varepsilon_{ij}(\omega,\mathbf{k})$ includes both electric and magnetic responses, since **E** and **B** are related by $\nabla \times \mathbf{E} = -(\partial \mathbf{B}/\partial t)/c$. The dependence of **D** on **B** can be equivalently treated as a dependence of **D** on the spatial derivative of **E**; i.e., a permittivity with spatial dispersion takes good care of both fields. Thus, it does not lose generality to set $\mu_{ij}(\omega) = \delta_{ij}$ [16].

In the simple case, permittivity and permeability depend only on frequency, since we assume that the local electric polarization at a point is decided only by the field at that point. From the Fourier transform

$$E_i(\omega,\mathbf{k}) = \frac{1}{(2\pi)^4}\int dt \int d\mathbf{r} E_i(\mathbf{r},t)\exp[-i(\mathbf{k}\cdot\mathbf{r}-\omega t)] \tag{1}$$

and the constitutive relation

$$D_i(\omega,\mathbf{k}) = \varepsilon_{ij}(\omega,\mathbf{k})\, E_j(\omega,\mathbf{k}), \tag{2}$$

we can see that, when the field is not strictly local, the dependence of the field on **r** corresponds to the dependence of permittivity on **k** in the frequency domain. The inclusion of the spatial dispersion is also a natural requirement to

study longitudinal waves, since otherwise the group velocity of the longitudinal waves goes to zero [16].

The general form of the dielectric tensor in optical crystals with spatial dispersion [28] is written as

$$\varepsilon_{ij}(\omega,\mathbf{k}) = \varepsilon_{ij}(\omega) + \alpha_{ijlm}(\omega)k_l k_m, \tag{3}$$

which comes as a Taylor expansion with the correction of the spatial terms, and the first nonzero terms are to the second order of $\mathbf{k}$. The zeroth-order term $\varepsilon_{ij}(\omega)$ is substituted with the plasma permittivity

$$\varepsilon_p(\omega) = 1 - \omega_p^2/\omega^2, \tag{4}$$

since a 3D wire array is shown to be plasmalike in the gigahertz range [2]. ω_p is evaluated as the cutoff angular frequency (the corresponding frequency $f_p = 17.7$ GHz). Note that, in this paper, all the equations are in Gaussian units, and the Einstein summation notation is used.

We propose a trial solution of the permittivity tensor

$$\varepsilon_{ij}(\omega,\mathbf{k}) = \begin{cases} \varepsilon_p(\omega) + \frac{\alpha_1 k_i^2 c^2 + \sum_{l\neq i}\alpha_2 k_l^2 c^2}{\omega^2-\omega_p^2} & (j=i), \\ \frac{2\alpha_3 k_i k_j c^2}{\omega^2-\omega_p^2} & (j\neq i), \end{cases} \tag{5}$$

to use in the Maxwell equations in Gaussian units describing electromagnetic fields in a medium

$$\begin{aligned} \nabla\cdot\mathbf{B} &= 0, \\ \nabla\cdot\mathbf{D} &= 4\pi\rho_0, \\ \nabla\times\mathbf{E} &= -\frac{1}{c}\partial\mathbf{B}/\partial t, \\ \nabla\times\mathbf{B} &= \frac{1}{c}\partial\mathbf{D}/\partial t + \frac{4\pi}{c}\mathbf{j}_0. \end{aligned} \tag{6}$$

The pole we put in the α_{ijlm} terms is similar to that of the quadrupole transition of an exciton between two states [28]. Near a dipole transition, we have

$$\varepsilon(\omega) = \varepsilon_0 - \frac{\Omega_0^2}{\omega^2-\omega_{0s}^2}, \tag{7}$$

where $\omega_{0s} = \omega_s - \omega_0$ is the frequency difference between the two states and $\Omega_0^2 = \text{const}\cdot|\int\psi_s^*\mathbf{r}\psi_0 d\mathbf{r}|^2$, where ψ represents the wave functions of the two states. For a quadrupole mode, the Ω_0^2 changes to $\text{const}\cdot|\int\psi_s^*\mathbf{r}(\mathbf{k}\cdot\mathbf{r})\psi_0 d\mathbf{r}|^2$, so near the quadrupole line, the permittivity has the form of

$$\varepsilon(\omega,\mathbf{k}) = \varepsilon_0 - \frac{\text{const}\cdot k^2}{\omega^2-\omega_{0s}^2}. \tag{8}$$

Then we decide the remaining parameters α_1, α_2, and α_3 from fitting the dispersion curves calculated with the following wave equation derived from Eq. (6) in the special case of no free charge or current:

$$\det\left(\frac{\omega^2}{c^2}\varepsilon_{ij} - k^2\delta_{ij} + k_i k_j\right) = 0. \tag{9}$$

Figure 4 shows the fitting results and the best fit of α_1, α_2, and α_3. In the Γ-X region, the modes of interest (mode 1 and mode 3) are modeled well, and they are nearly straight lines with slopes proportional to $\pm\sqrt{-\alpha_1}$ with $|\alpha_1| \ll 1$. For the dispersion in the $\Gamma - X$ region of mode 4, the assumption of treating the structure as a homogeneous medium is not as good as for the lower modes due to a smaller wavelength. However, modes 1 and 3 are important to the interaction of an electron beam with the wave, so the quality of this fit, which is very good, is important. The same number of modes and similar changing patterns with frequency are not easily achieved by establishing an analytical model without the introduction of spatial dispersion. Spatial dispersion is not a slight correction here but makes qualitative differences. This can happen when a pole exists, since the dispersion relation is modified most drastically in the vicinity of the pole, as even a small $\mathbf{k}$ can change the permittivity significantly, and additional roots of the dispersion equation may appear [28].

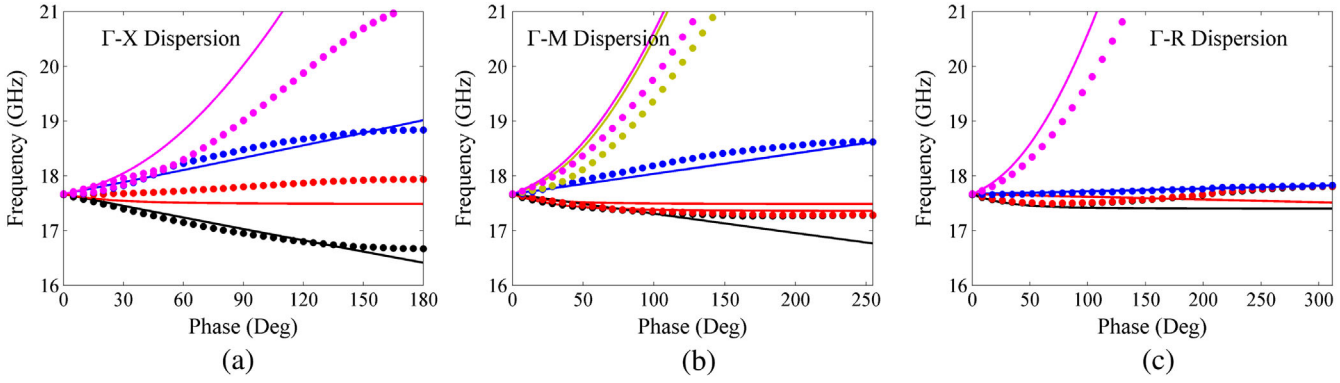

FIG. 4. Fitting results of the dispersion curves. HFSS results are in dotted lines, and the fitting curves are in solid lines. The optimized parameters are $\alpha_1 = -0.0209$, $\alpha_2 = -0.0209$, and $\alpha_3 = 0.0156$. (a) $\Gamma - X$. (b) $\Gamma - M$. (c) $\Gamma - R$. Modes 1, 2, 3, and 4 are denoted with black, red, blue, and magenta, respectively. In the $\Gamma - M$ region, mode 4 splits into two modes.

IV. WAVE-BEAM INTERACTION USING THE EFFECTIVE MEDIUM THEORY

Next, we study the interaction of the volumetric MTM structure with a relativistic beam. Theoretically, we can use the effective medium theory to predict the energy loss of the beam due to radiation. Suppose a point charge moves in the x direction at $\mathbf{v} = v\mathbf{e}_x$ into the effective homogeneous medium. The charge and current densities are $\rho_0(\mathbf{r}, t) = q\delta(\mathbf{r} - \mathbf{v}t)$ and $\mathbf{j}_0(\mathbf{r}, t) = qv\delta(\mathbf{r} - \mathbf{v}t)\mathbf{e}_x$, respectively. From the Maxwell equations as Eq. (6), the equation for $E(\omega, \mathbf{k})$ is

$$E_i(\omega, \mathbf{k}) = i\frac{4\pi\omega}{c^2}A_{ij}^{-1}j_{0j}(\omega, \mathbf{k}), \tag{10}$$

where A is a matrix whose element A_{ij} is

$$A_{ij} = k^2\delta_{ij} - k_ik_j - \frac{\omega^2}{c^2}\varepsilon_{ij}. \tag{11}$$

The current of the point charge in the frequency domain is

$$\begin{aligned} j_{0j}(\omega, \mathbf{k}) &= \frac{qv_j}{(2\pi)^4}\int dt \int d\mathbf{r}\delta(\mathbf{r} - \mathbf{v}t)\exp[-i(\mathbf{k}\cdot\mathbf{r} - \omega t)] \\ &= \frac{qv_j}{(2\pi)^3}\delta(\omega - \mathbf{k}\cdot\mathbf{v}). \end{aligned} \tag{12}$$

Note that only v_x is nonzero, so

$$E_x(\omega, \mathbf{k}) = \frac{iq\omega v}{2\pi^2c^2}A_{xx}^{-1}\delta(\omega - k_xv). \tag{13}$$

Then we inverse transform the $\mathbf{k}$ space back to the $\mathbf{r}$ space. The frequency spectrum $E_x(\omega, \mathbf{r})$ on the beam trajectory with $y = z = 0$ is

$$\begin{aligned} &E_x(\omega, \mathbf{r})\Big|_{y=z=0} \\ &= -\frac{q\omega}{2\pi^2c^2}\iint dk_ydk_z\mathrm{Im}\left[\exp\left(i\frac{\omega x}{v}\right)A_{xx}^{-1}\right]\Bigg|_{k_x=\omega/v}. \end{aligned} \tag{14}$$

The integrands become peaked when $|A_{xx}^{-1}|$ has a resonance, and the peaks mean that electromagnetic waves are excited by the moving charge [29]. We consider the loss in the effective medium model by changing the denominators in the spatial dispersion terms from $\omega^2 - \omega_p^2$ to $\omega^2 - \omega_p^2 + i\gamma_l\omega$, where the $i\gamma_l\omega$ term represents a small Ohmic loss and $\gamma_l \ll \omega_p$. We calculate $E_x(\omega, \mathbf{r})|_{y=z=0}$ numerically and find two peaks at 16.6 and 19.1 GHz when v is close to c. These frequencies agree well with the frequencies calculated using HFSS, as shown in Table I below. Since the energy loss of the charge in the medium per unit path length is decided by $W = q(\mathbf{v}\cdot\mathbf{E})/v$ at $\mathbf{r} = \mathbf{v}t$, these frequencies are also where the beam loses energy most intensively to the radiated field. This energy loss is caused by longitudinal modes (plasmons) only, and there is no velocity threshold in this case unlike the condition for normal CR.

TABLE I. Comparison of wave-beam interaction frequencies (unit, GHz).

	HFSS eigenmode solver	Effective medium theory	CST wakefield solver
Mode 1	16.7	16.6	16.6
Mode 3	18.8	19.1	18.7

To test the above result, we use the CST wakefield solver to simulate fields radiated by a passing beam. The beam in the wakefield solver is represented with a line current with a longitudinally Gaussian shaped charge. The model is set up with periodic boundaries on the side walls and 36 cells in the beam propagating direction. So the actual structure is an array of the unit cells infinite in the transverse directions resembling a homogeneous medium.

The wake potentials generated by a bunch with charge q at a distance of s behind it can be expressed as [30]

$$\begin{aligned} \mathbf{W}(y, z, s) = \frac{1}{q}\int_{-\infty}^{\infty}\Bigg[&\mathbf{E}\left(x, y, z, t = \frac{s + x}{v}\right) \\ &+ \frac{\mathbf{v}}{c}\times\mathbf{B}\left(x, y, z, t = \frac{s + x}{v}\right)\Bigg]dx, \end{aligned} \tag{15}$$

and the longitudinal wake impedance is defined by

$$Z_x(\omega) = \frac{1}{c}\int_{-\infty}^{\infty}W_x(s)\exp(-i\omega s/c)ds. \tag{16}$$

We can simulate the wake impedance with the CST code, and Fig. 5 shows the simulated spectrum of the structure with an infinite array of cells in the transverse direction.

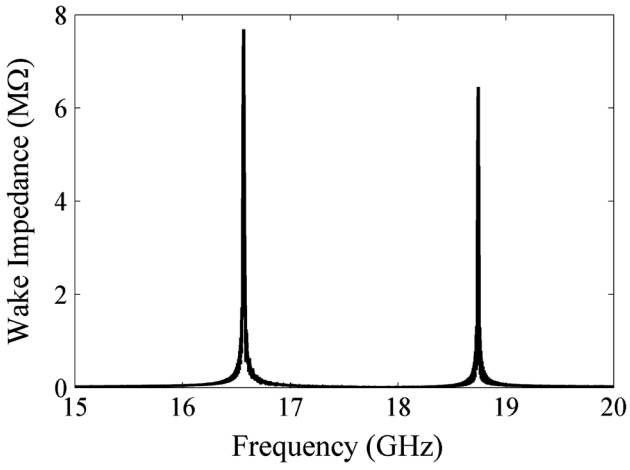

FIG. 5. Longitudinal wake impedance spectrum. Peaks are located at 16.6 and 18.7 GHz, corresponding to eigenmode 1 and 3, respectively.

For this simulation, we have used a 1 pC charge bunch traveling at the speed of light with a FWHM length of 2 mm. The peak interaction frequency points agree very well with the results of the effective medium theory, as shown in Table I. Thus, the effective medium model successfully locates the interaction frequencies.

V. RADIATION PATTERN IN A VOLUMETRIC ARRAY OF MTM UNIT CELLS

In reality, we need a finite-size structure, so the simulation in CST is then performed by simulating the transmission of a relativistic beam through an array of the unit cells. The radiation pattern is naturally complicated by two additional effects. First, the microstructure of the unit cells prevents the whole structure from acting strictly as a homogeneous medium, so, when the beam passes through the inhomogeneous regions, transition radiation happens in addition to the CR. Second, the structure is metallic, so it will deform the radiated field by imposing boundary conditions at metal walls.

We group the unit cells into an array as shown in Fig. 6(a). Cell numbers in the x, y, and z directions are 10, 7, and 7, respectively. The beam travels through the central line along the $+x$ direction. Perfect absorbing boundaries are imposed at a distance of 7 cells away from the structure in the x, y, and z directions. This setup enables us to study the radiation pattern in the bulk structure in an unbounded state.

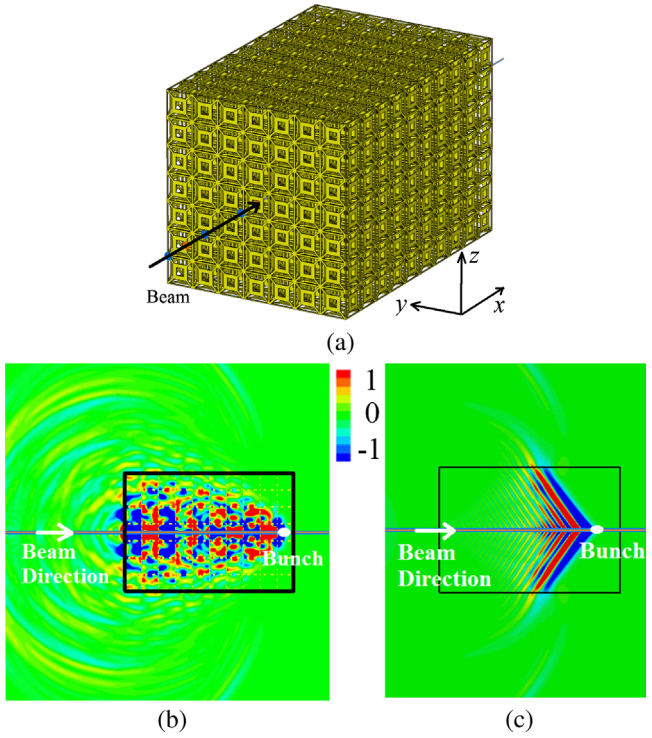

FIG. 6. Radiation pattern with a relativistic beam. (a) Illustration of the bulk structure. The beam passes through the line of $y = z = 0$. (b) Longitudinal E field (E_x) on $y = 0$ middle cutting plane for the MTM structure. The MTM region is enclosed in the black rectangles. (c) The same result for the volume mode of a dielectric with $\varepsilon = 1.5$.

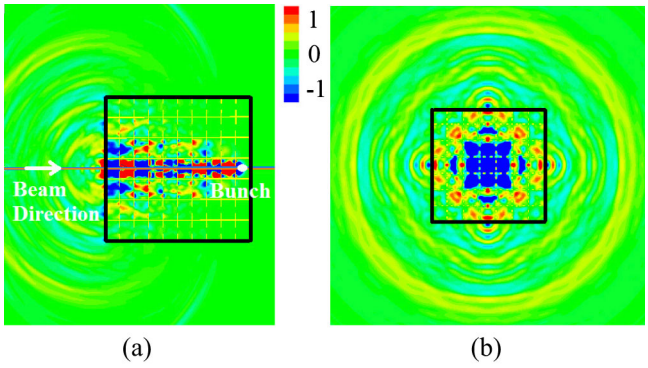

FIG. 7. The 3D properties. (a) Radiated E_x field on an oblique cutting plane rotated 45° around the x axis starting from the $y = 0$ plane. (b) Radiation pattern on the cutting plane of $x = \text{const}$; i.e., the cutting plane is perpendicular to the longitudinal direction.

Figure 6(b) shows the pattern of radiated longitudinal electric field E_x in the middle cutting plane ($y = 0$ plane). As a comparison, we show the radiation pattern in a volume of the same shape but built with a dielectric of $\varepsilon = 1.5$ in Fig. 6(c). In the MTM case, electromagnetic energy goes backward, until the waves exit the structure at the same end where the beam enters. However, in the case of radiation in the dielectric medium, as in Fig. 6(c), electromagnetic energy travels forward, as is expected in conventional CR.

Since the unit cell has the feature of 3D negative group velocity, we can observe backward radiation in directions different from the coordinate axes. Figure 7(a) shows the field on the cutting plane which is rotated 45° from the $y = 0$ plane around the beam axis. This plane and the $y = 0$ plane are not symmetric geometrically, but a similar pattern of backward radiation is observed. Figure 7(b) shows the E_x pattern on a cutting plane perpendicular to the x direction. The MTM structure itself is not isotropic, but the waves grow as isotropic, nearly spherical wave fronts when they enter the vacuum region. So, when the beam goes through the volumetric structure, a cone is formed behind it in the vacuum region where wave fronts are spherical-like and propagate backward.

VI. WAKEFIELD ACCELERATION

When a bunch travels through the structure, wakefields are generated by the CR mechanism, and this leads to the possible application of wakefield acceleration. The scheme of wakefield acceleration is that an intense electron drive bunch excites wakefields which can be used to accelerate a following witness bunch with a smaller charge [31], and the system is generally a dielectric-lined waveguide [32–34]. The MTM structure can operate in a manner similar to the dielectric wakefield acceleration regime but with only

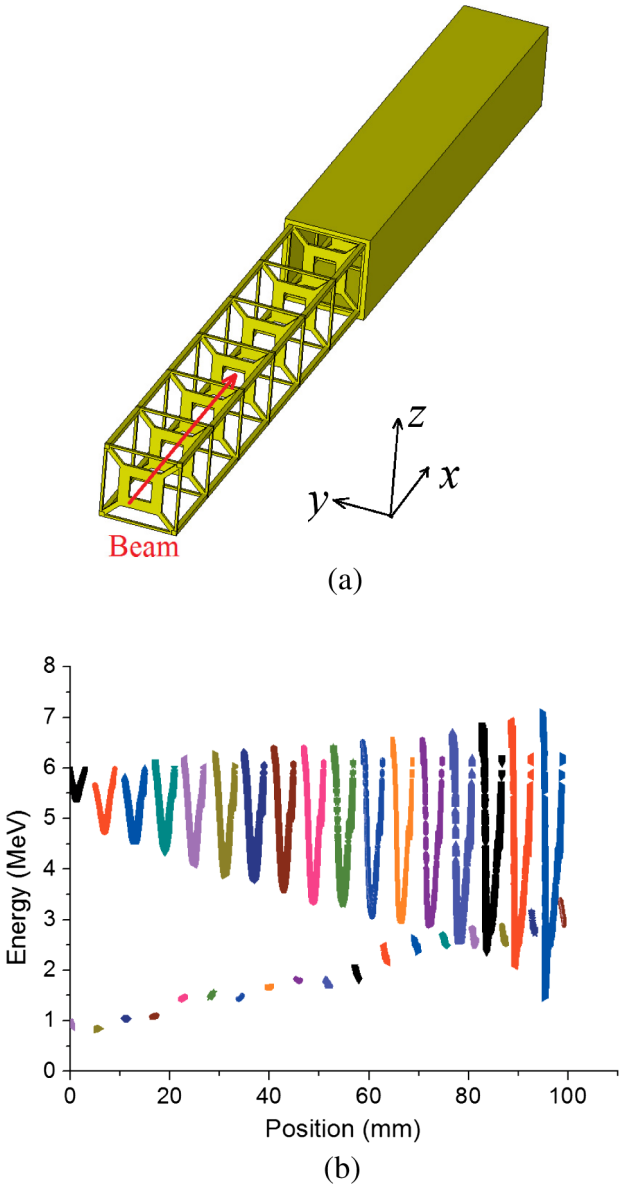

FIG. 8. (a) Structure for wakefield acceleration demonstration. Part of the waveguide is removed to show the inside structure. (b) Phase space evolution in the x direction of the drive bunch (the top group) and the witness bunch (the bottom group). The time interval between every two snapshots is 0.02 ns. The plots of the two bunches at the same time are represented with the same color. The witness bunch is injected into the structure 25 mm after the drive bunch.

metal. This has the potential advantage of producing a more rugged structure and a structure that does not suffer from dielectric breakdown effects.

To fit the structure in a waveguide, we modify the unit cell from six-face cubic to two faces supported by four rods, as shown in Fig. 8(a). 12 unit cells are aligned in a single row inside a waveguide. The coupling slots lock the frequency below the cutoff frequency of the waveguide. The eigenmode simulation shows that the cutoff frequency of the MTM structure shown in Fig. 8(a) is 17.5 GHz.

The electron beams consist of a drive bunch and a witness bunch going through the central line in the $+x$ direction. The drive bunch is a Gaussian bunch of FWHM length 2 mm carrying a charge of 40 nC, and the witness bunch carries 1 pC and is 0.4 mm long. The spacing of the witness bunch behind the drive bunch is optimized to 25 mm to achieve the maximum average accelerating gradient. The drive bunch has an initial energy of 6 MeV, and the witness bunch 1 MeV.

Figure 8(b) shows the evolution of the two bunches in phase space. The drive bunch keeps losing energy to electromagnetic waves in the structure until it exits the structure, and the witness bunch is accelerated from 1 to 3.1 MeV. This corresponds to an average accelerating gradient of 21 MV/m on the witness bunch path.

VII. CONCLUSIONS

In this paper, we present the design of a metallic MTM unit cell that can be used to fill all of space. The cell size is scaled to work for 17 GHz and can be easily scaled to other frequencies. Of all the eigenmodes of the unit cell, the mode with negative group velocity is the lowest-order mode and shows a longitudinal electric field pattern. Theoretically, we have proved that a homogeneity approximation with spatial dispersion accurately describes the dispersion characteristics. Spatial dispersion yields a strong modification to the dispersion curves instead of a small modification, as additional modes appear. When interacting with relativistic electron beams, the MTM structure shows a backward radiation pattern. The wakefield generated by a drive bunch can be used to accelerate a following witness bunch.

ACKNOWLEDGMENTS

This research was supported by the U.S. Department of Energy, Office of Science, Office of High Energy Physics under Award No. DE-SC0010075 and the Air Force Office of Scientific Research under MURI Grant No. FA 550-12-1-0489.

[1] V. G. Veselago, Sov. Phys. Usp. **10**, 509 (1968).
[2] R. Marqués, F. Martín, and M. Sorolla, *Metamaterials with Negative Parameters: Theory, Design and Microwave Applications* (Wiley, New York, 2011).
[3] S. A. Ramakrishna and T. M. Grzegorczyk, *Physics and Applications of Negative Refractive Index Materials* (CRC, Boca Raton, 2009).
[4] D. Schurig, J. J. Mock, B. J. Justice, S. A. Cummer, J. B. Pendry, A. F. Starr, and D. R. Smith, Science **314**, 977 (2006).
[5] J. B. Pendry, Phys. Rev. Lett. **85**, 3966 (2000).

[6] A. K. Iyer and G. V. Eleftheriades, Appl. Phys. Lett. **92**, 131105 (2008).

[7] S. Enoch, G. Tayeb, P. Sabouroux, N. Guérin, and P. Vincent, Phys. Rev. Lett. **89**, 213902 (2002).

[8] S. Antipov, L. Spentzouris, W. Liu, W. Gai, and J. G. Power, J. Appl. Phys. **102**, 034906 (2007).

[9] S. Antipov, L. Spentzouris, W. Gai, M. Conde, F. Franchini, R. Konecny, W. Liu, J. G. Power, Z. Yusof, and C. Jing, J. Appl. Phys. **104**, 014901 (2008).

[10] M. A. Shapiro, S. Trendafilov, Y. Urzhumov, A. Alù, R. J. Temkin, and G. Shvets, Phys. Rev. B **86**, 085132 (2012).

[11] J. S. Hummelt, S. M. Lewis, M. A. Shapiro, and R. J. Temkin, IEEE Trans. Plasma Sci. **42**, 930 (2014).

[12] D. R. Smith, D. C. Vier, Th. Koschny, and C. M. Soukoulis, Phys. Rev. E **71**, 036617 (2005).

[13] S. Arslanagic, T. V. Hansen, N. A. Mortensen, A. H. Gregersen, O. Sigmund, R. W. Ziolkowski, and O. Breinbjerg, IEEE Antennas Propag. Mag. **55**, 91 (2013).

[14] X. Chen, T. M. Grzegorczyk, B. I. Wu, J. Pacheco, and J. A. Kong, Phys. Rev. E **70**, 016608 (2004).

[15] Z. Duan, J. S. Hummelt, M. A. Shapiro, and R. J. Temkin, Phys. Plasmas **21**, 103301 (2014).

[16] L. D. Landau and E. M. Lifshits, *Electrodynamics of Continuous Media* (Butterworth-Heinemann, London, 1984).

[17] V. M. Agranovič, Y. R. Shen, R. H. Baughman, and A. A. Zakhidov, Phys. Rev. B **69**, 165112 (2004).

[18] A. Demetriadou and J. B. Pendry, J. Phys. Condens. Matter **20**, 295222 (2008).

[19] M. A. Shapiro, G. Shvets, J. R. Sirigiri, and R. J. Temkin, Opt. Lett. **31**, 2051 (2006).

[20] V. M. Agranovič and Y. N. Gartstein, Phys. Usp. **49**, 1029 (2006).

[21] W. C. Haxton, Phys. Rev. D **36**, 2283 (1987).

[22] A. Grbic and G. V. Eleftheriades, J. Appl. Phys. **92**, 5930 (2002).

[23] J. Lu, T. M. Grzegorczyk, Y. Zhang, J. Pacheco, B. I. Wu, J. A. Kong, and M. Chen, Opt. Express **11**, 723 (2003).

[24] Z. Duan, B. I. Wu, J. Lu, J. A. Kong, and M. Chen, Opt. Express **16**, 18479 (2008).

[25] B. I. Wu, J. Lu, J. A. Kong, and M. Chen, J. Appl. Phys. **102**, 114907 (2007).

[26] S. Xi, H. Chen, T. Jiang, L. Ran, J. Huangfu, B. I. Wu, J. A. Kong, and M. Chen, Phys. Rev. Lett. **103**, 194801 (2009).

[27] V. V. Vorobev and A. V. Tyukhtin, Phys. Rev. Lett. **108**, 184801 (2012).

[28] V. M. Agranovič and V. L. Ginzburg, *Crystal Optics with Spatial Dispersion, and Excitons* (Springer, New York, 1984).

[29] A. F. Alexandrov, L. S. Bogdankevich, and A. A. Rukhadze, *Principles of Plasma Electrodynamics* (Springer-Verlag, Berlin, 1984).

[30] T. P. Wangler, *RF Linear Accelerators* (Wiley, New York, 2008).

[31] W. Gai, P. Schoessow, B. Cole, R. Konecny, J. Norem, J. Rosenzweig, and J. Simpson, Phys. Rev. Lett. **61**, 2756 (1988).

[32] T. B. Zhang, J. L. Hirshfield, T. C. Marshall, and B. Hafizi, Phys. Rev. E **56**, 4647 (1997).

[33] A. M. Cook, R. Tikhoplav, S. Y. Tochitsky, G. Travish, O. B. Williams, and J. B. Rosenzweig, Phys. Rev. Lett. **103**, 095003 (2009).

[34] G. Andonian, D. Stratakis, M. Babzien, S. Barber, M. Fedurin, E. Hemsing, K. Kusche, P. Muggli, B. O'Shea, X. Wei, O. Williams, V. Yakimenko, and J. B. Rosenzweig, Phys. Rev. Lett. **108**, 244801 (2012).